RSC Advances

ROYAL SOCIETY OF CHEMISTRY

www.rsc.org/advances

Graphical abstract

A facile procedure for immobilizing and photopatterning amino ligands onto a multilayer cross-linked COOH-functionalized organosilica film is described. Key features include high functionality, robustness and no restriction on substrate.

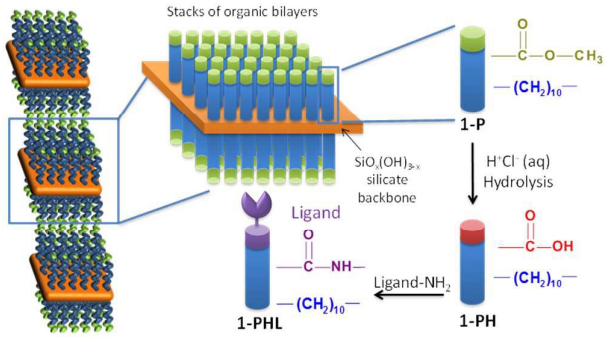

Journal Name

RSCPublishing

ARTICLE

Photoinduced Self-assembly of Carboxylic Acid-Terminated Lamellar Silsesquioxane: Highly Functional Films for Attaching and Patterning Amino-Based Ligands

Cite this: DOI: 10.1039/x0xx00000x

Received 00th January 2012,
Accepted 00th January 2012

DOI: 10.1039/x0xx00000x

www.rsc.org/

Lingli Ni,[*ad] Abraham Chemtob,[*a] Céline Croutxé-Barghorn,[a] Céline Dietlin,[b] Jocelyne Brendlé,[b] Séverinne Rigolet,[b] Loïc Vidal,[b] Alain Dieterlen,[c] Elie Maalouf,[c] and Olivier Haeberlé[c]

Recently, long *n*-alkyltrimethoxysilanes ($H_3C(CH_2)_nSi(OCH_3)_3$) have proven to self-assemble into mesoscopically ordered passive lamellar films through an efficient solvent-free photoacid-catalysed sol-gel process. By using an analogue precursor architecture presenting terminal ester group ($H_3COC(O)(CH_2)_{10}Si(OCH_3)_3$), both functional and tuneable nanostructured organosilica films were synthesized, while keeping all processing advantages of light-induced self-assembly. The subsequent attachment of a fluorescent amino-based ligand (Safranin O) was performed using a two-step procedure. The ester end groups were first hydrolysed in reactive carboxylic using standard methods, and activated with an amino ligand to form amide bonds. Hydrolysis and ligand coupling were assessed through infrared and solid-state ^{1}H NMR spectroscopy. Direct patterning of the fluorescent ligand-functionalized silsesquioxane film was performed by exposure to deep UV under a mask to cause the local degradation of the dye. The resultant photopatterned film was detected using fluorescence microscopy. This UV method could represent an effective and general approach for attaching and patterning amino-based ligands, with less restriction on substrate and surface preparation than self-assembled monolayers.

1. Introduction

Hybrid sol-gel silicates derived from silsesquioxane precursors, R-$[Si(OR')_3]_n$ ($n \geq 1$), where R and OR' are respectively covalently attached organic groups and hydrolyzable alkoxy functions, represent a highly versatile class of nanocomposites.[1, 2] In the early development phase, the reported hybrids were amorphous, and their growth was essentially driven by the inexhaustible choice of organic moieties achieved through the Si-C bond molecular scale homogeneity. More recently, research efforts have centred on ways to inhibit the disordering effect of Si-O-Si condensation, in order to create ordered organosilica nanostructures.[3, 4] Harnessing silsesquioxanes in a way that the organic and siloxane fragments self-assemble into spatially defined and organized nanodomains has been a very attractive goal to fabricate a wide spectrum of advanced hybrid nanomaterials including membranes,[5] conductive films,[6] absorbents[7] and optoelectronic devices.[8] In fact, unique chemical or physical properties may emerge from hybrid materials when organic moieties form mesoscopically segregated functional domains, both ordered and confined.[9]

When the ultimate aim is not the fabrication of mesoporous materials, the major route for synthesizing nanostructured hybrids has been the direct template-free self-assembly of silsesquioxane precursors, usually leading to lamellar structures. Critical to self-organization is the presence of noncovalent binding organic groups (van der Waals forces, π-π stacking) or/and amphiphilic interactions. This has imposed strict constraints on precursor architecture and synthesis conditions, which account for the fact that the long-range molecular ordering of most organosilica hybrids has remained very challenging.[10] Accordingly, self-assembled hybrids rely only on a handful of mono-, bis- or multi-silylated building blocks picked essentially for driving self-assembly. To this end,

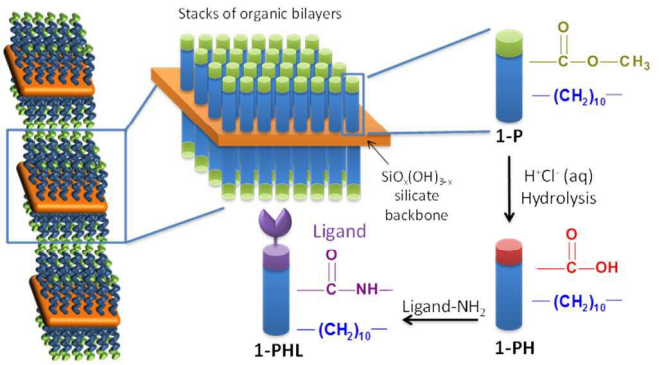

Figure 1. Supramolecular structure formed by the photoinduced self-assembly of precursor **1**.

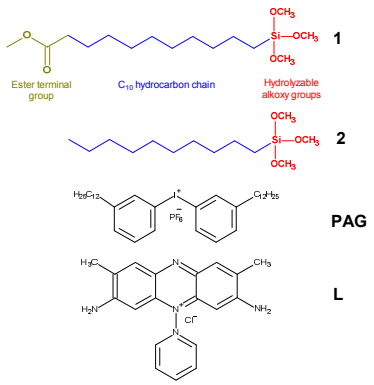

Scheme 1. Structures of monosilylated trimethoxysilane precursors (**1**, **2**), photoacid generator (**PAG**) and fluorescent amino-based ligand (**L**)

the suitable organic moieties R must be able to develop hydrophobic interactions (long hydrocarbon chain[11]) or/and hydrogen bonds (ureido[12], amide groups[13]). Notwithstanding the wealth of periodically ordered mesostructures achieved with these precursors, they have actually a narrow application potential due to restricted intrinsic functionality. For hybrids to fully benefit from nanostructuration, there is the need of simple organic groups, not only tolerant or favourable to self-assembly, but also able to confer functionality and specific properties to the final material. There have been very few examples of such 'active' nanostructured silsesquioxanes, containing for example photosensitive (azobenzene,[14] diacetylene,[15] perylenediimide[16]) or conductive organic groups (crown ether,[17] perylene[18-20]). Recently, Mehdi et al. reported several multi-step routes to yield amino-, thiol-[21], sulfonic acid-[21], carboxylic acid-[22-25] and phosphonic acid-[23] functionalized lamellar hybrids. The high density of reactive and accessible end groups arranged within a robust lamellar mesostructure was exploited for the chelation of transition metals and lanthanides in separation applications.[3] Despite the success of this methodology, all the reported materials lacked uniform morphology control.

In this work, we report an efficient UV-driven approach to COOH-functionalized lamellar organosilica films with long-range molecular ordering and uniform film morphology via a photoacid-catalysed sol-gel process. Using this original approach, we have recently described the formation of 'passive' lamellar alkyl silicate films[26, 27] and its mechanism.[28] UV control offers several advantages over conventional sol-gel process such as storable, ready-to-use formulation with no pot-life issue since the photocatalyst (superacid) is released on demand. Additionally, photopolymerization helps to make the process faster, solvent-free and energy-saving. Here, a similar UV-mediated methodology is exploited to synthesize, for the first time, functional multilayer silsesquioxane films.

Introduction of carboxylic acid groups into the supramolecular structure is based on a 2-step procedure, as outlined in Figure 1. Scheme 1 shows the structure of the starting ester-terminated trimethoxysilane precursor **1** ($H_3COC(O)(CH_2)_{10}Si(OCH_3)_3$) derived from a purely aliphatic precursor ($H_3C(CH_2)_9Si(OCH_3)_3$, **2**). Upon UV irradiation in the presence of photoacid generator (**PAG**, Scheme 1), this precursor film condenses into a mesoscopically ordered and cross-linked lamellar architecture. Hydrophobic interactions ($C_{10}H_{21}$) combined with hydrogen bonds (CH_2-C=O, Si-OH) serve to self-assemble precursor **1**. Subsequently, the terminal ester groups of this robust structure can be partially hydrolyzed into carboxylic acid groups without undermining the mesostructural order. In our case, we chose precursor **1** because of the high abundance of useful amino-based ligands in chemistry, which can be conjugated in high yield to the resultant carboxylic acid groups. To illustrate the usefulness of the method, we used Safranin O, a fluorescent amino ligand (**L**, Scheme 1) mimicking for example biologically relevant amino derivative ligands able to bind proteins or promote the adhesion of mammalian cells.[29, 30] The first advantage of this prototype system is that ligand's retention and binding onto the lamellar hybrid mesostructure can be readily confirmed by optical and fluorescence imaging. Another key feature of **L** includes its facile spatially-controlled decomposition when exposed to deep UV light under a photomask, in order to generate precisely defined and easy characterized fluorescent patterns.

2. Experimental Section

2.1 Chemicals

Methyl 11-(trimethoxysilyl)undecanoate (**1**, 95 mol. %), *n*-decyltrimethoxysilane (**2**, 98 mol. %) were purchased from SIKÉMIA and ABCR, respectively. The bis-dodecyl diphenyliodonium hexafluoroantimonate salt (UV1241) **PAG** was provided by Deuteron. Hydrochloric acid (36.5-38 mol. %), acetonitrile (99.8 mol. %) and Safranin O (**L**, 85 mol. %) were supplied by Sigma-Aldrich. Technical acetone and ethanol were provided by Carlo Erba and VWR respectively. All the chemicals were used as received without further purification.

2.2 Synthesis of ester- and carboxylic acid-functionalized silsesquioxane lamellar films

2 wt. % of **PAG** was dissolved in precursor **1** to form a photolatent homogeneous mixture. The resultant nonhydrolysed

solution was coated on a silicon wafer using an automatic film applicator (Elcometer 4340) equipped with a wire wound bar to yield a ca. 2 µm thick liquid film. Subsequent ambient UV irradiation was performed, at room temperature and ambient humidity (30-35 %), using a medium-pressure Hg-Xe lamp (Hamamatsu L8252, 365 nm reflector) coupled with a flexible light-guide, at a controlled irradiance of 20 mW/cm^2 (the emission spectrum of the UV lamp is provided in the supplementary information, Fig. S1). The film samples were irradiated during 1800 s to yield transparent solid ester-functionalized silsesquioxane film (**1-P**). The as-synthesized coated nanocomposite was immersed in an HCl aqueous solution (50 mL, 2 mol/L) at 65°C without stirring for 18 h to promote the conversion of the ester functions into carboxylic acids. The resultant film (**1-PH**) was thoroughly rinsed with deionized water until the pH of the washing solution remained within the range of 6 to 7. The as-synthesized film was dried overnight in vacuum at room temperature.

2.3 Coupling of the carboxylic acid-functionalized silsesquioxane film with an amino fluorescent ligand and its deep UV photopatterning

The substrate coated with acid-terminated silsesquioxane (**1-PH**) was activated by immersion in a solution of acetonitrile (50 mL) with Safranin O (**L**, 0.01 mol/L). 12 h exposure converted the transparent colourless film into a red film (**1-PHL**). Several washings of the film with acetonitrile were performed until the characteristic signature of Safranin O (maximum absorption at λ_{max} = 517 nm) became non detectable in UV-vis spectroscopy (1 cm thick quartz cell). The **1-PHL** film was rinsed with deionized water and vacuum dried at room temperature for 24 h. Subsequently, a TEM grid was deposited onto the solid film surface, and was eventually exposed during 1 hour to deep UV light provided by a medium-pressure Hg-Xe lamp (Hamamatsu L8252, 254 nm reflector). This lamp was connected to a flexible light-guide generating a focused light beam on the film sample. Under these irradiation conditions, the flux of energetic photons is high enough (irradiance = 80 mW/cm^2 for λ < 300 nm and 600 mW/cm^2 for the whole UV spectrum) to enable the degradation of the organic ligand. Finally, the TEM grid was removed showing a red/transparent micropatterned film indicative of a spatially-controlled photodegradation. The sample was washed several times with ethanol and acetone to remove the organic fragments expelled from the film during photocalcination.

2.4 Characterization

Infrared spectra obtained by FTIR spectroscopy were recorded with a Bruker Vertex 70. The resolution of the infrared spectra was 2 cm^{-1}. For all experiments, an effective precursor **1** film thickness of 2 µm was chosen and assessed by profilometry using an Altisurf 500 workstation (Altimet) equipped with a 350 µm AltiProbe optical sensor. X-Ray Diffraction patterns (XRD) were obtained on a PANalytical X'pert Pro diffractometer with fixed slits

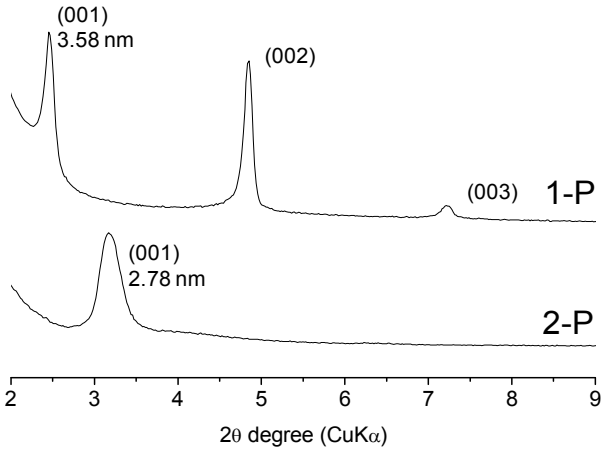

Figure 2. XRD patterns for the two nanocomposite films (**1-P** and **2-P**) assembled from **1** and **2**.

using Cu/Kα radiation (λ = 1.5418 Å) and θ-2θ mounting. Before analysis, films on silicon wafers were directly deposed on a stainless steel sample holder. Data were collected between 1 and 10 ° 2θ degrees (XRD) with a scanning step of 0.01° s^{-1}. Morphologies of the samples were characterized by scanning electron microscopy (SEM) (FEI Quanta 400 microscope working at 30 kV). The samples being nonconductive, they have been metalized with gold (15 nm thickness). ^{1}H (I = 1/2) MAS NMR experiment was performed at room temperature on a Bruker Avance II 400 spectrometer operating at B_0 = 9.4 T (Larmor frequency ν_0 = 400.17 MHz). Single pulse experiment was recorded with a double channel 2.5 mm Bruker MAS probe, a spinning frequency of 25 kHz, a π/2 pulse duration of 3.5 µs and a 10 s recycling delay. 64 scans were recorded. Optical observations of the photopolymerized films were performed using an Olympus BX51 microscope in fluorescence modes. The microscope is equipped with U-LH75XEAPO Argon lamp. Fluorescence excitation is performed through a FITC block filter U-MWIBA2 with an excitation filter BP460-490, a dichroic mirror DM505 and an emission filter BA510-550. Observation was performed at low magnification using 40x NA=0.65 Plan objectives, and at high magnification and high resolution using a 100x, NA=1,4 PlanApo oil-immersion objective. A CoolSnap HO^2 cooled camera is used for recording images. For precise and repetitive sample positioning, a Märzhäuser Wetzlar SCAN 130 x 85 2-D motorized stage is used. Accurate specimen focusing as well as three-dimensional measurements can be performed via motorized focusing controlled by the homemade software developed on ImageJ platform. Image processing (stacking, intensity and dimensional measurements) has been performed using the ImageJ software.

3. Results and discussion

3.1 Synthesis of self-assembled ester- and carboxylic acid-terminated silsesquioxane films

1 and **2** are two monosilylated silsesquioxane precursors (Scheme 1) having in common one trimethoxysilyl group

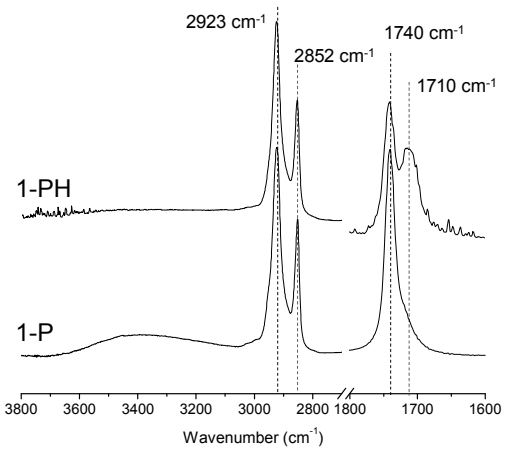

Figure 3. FTIR spectra of the silsesquioxane films **1-P** and **1-PH** obtained after 18 h immersion time in a 2 mol/L HCl aqueous solution at 65°C.

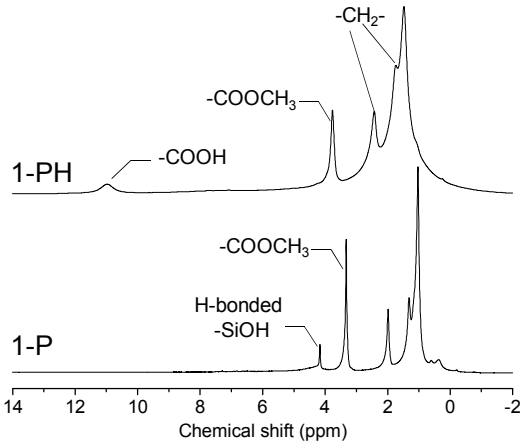

Figure 4. Solid state ^{1}H MAS NMR spectra of the hybrid films **1-P** and **1-PH** following ester hydrolysis

connected to a long C_{10} hydrocarbon chain. Such structural combination has recently proven to drive multilayer self-assembly through hydrophobic interactions.[28] Additionally, **1** has a tuneable methyl methanoate group ($H_3COC(=O)$-), thereby raising the question about the effect of this ester terminal group on supramolecular organization. Both precursors are commercially available, very stable in the open air and nonvolatile when they are in film form at ambient conditions. **1-** and **2**-based liquid films containing 2 wt. % of **PAG** were coated on silicon wafer substrate. Subsequent UV irradiation converted them into solid silsesquioxane films.

As shown in Figure 2, the XRD pattern of the hybrid films **1–P** and **2-P** derived respectively from **1** and **2** reflect the formation of highly ordered mesostructures. Regardless of the precursor, the long hydrophobic organic chains favoured low curvature mesophases, and the formation of lamellar structures with an intense (*001*) reflection. Additionally in **1-P**, the appearance of new (*002*) and (*003*) reflections (along with some peak narrowing) indicate a better ordering. This may be induced by additional hydrogen bonding between terminal CH_2-C=O moieties, which is the only structural difference between both precursors. Higher inter- and intramolecular interactions between organic groups can enhance the enthalpic association forces, and promote self-assembly. The corresponding d_{100} values are equal to 3.58 nm for **1-P** and 2.78 nm for **2-P**. These results are relatively consistent with the bilayer repeating unit distance $RSi(OH)_{3-x}O_x$---$O_x(OH)_{3-x}SiR$ (**1-P**: 3.52 nm and **2-P**: 3.14 nm) predicted by molecular models (using ChemDraw 3D calculation). This result therefore confirms the head-to-head bilayer packing of the lamellae, schematically shown in Figure 1. The film is made up of macroscopic multilayered crystallites with no specific orientation in contrast to Self-Assembled Monolayers (SAMs). Typically a few tens to a few hundreds of mesolayers may form spontaneously, but there was no estimate of the crystallite size. Furthermore, altering the aliphatic spacer with an ester end group has not affected the resulting mesophase. Accordingly, a longer hydrophobic pendant chain reduces the surfactant packing parameter, thus maintaining a lamellar organization in the film **2-P**. The FTIR spectrum of the nanocomposite derived from **1** (see the supporting information, Fig. S2) shows a quantitative consumption of the band corresponding to methoxysilyl functions ($\nu_s(SiOCH_3)$ ≈2840 cm^{-1}) within one minute. Moreover, based on the continuous growth of the Si-O-Si antisymmetric stretching band (1000-1260 cm^{-1}), we infer that photoinduced condensation reactions take place. However, there is no sign of ester groups' hydrolysis because the band at 1740 cm^{-1} (ν_{asym} of C=O groups) is unchanged (position, intensity) during and even after UV exposure. As a highly efficient reaction, we suggest that the superacid-catalysed hydrolysis of methoxysilyl groups may proceed through the permeation of only traces of atmospheric water.[31] Conversely, the acid-catalysed ester hydrolysis is an equilibrated reaction, which requires generally a much higher water concentration to shift the equilibrium towards products. Furthermore, the ester groups compartmentalized in the hydrophobic channel of the hybrid mesophases may not be accessible to the nucleophilic attack of water molecules, which on the contrary are localized preferentially in the hydrophilic siloxane interlayers.

However, heating the as-irradiated film **1-P** at 65°C in an acid HCl aqueous solution promotes the slow hydrolysis of the ester functions without damaging the aspect of the resultant film (**1-PH)**. Figure 3 shows the evolution of the IR spectrum in the carbonyl stretching region (1600-1800 cm^{-1}) after 18 h immersion. We see a significant decrease of the band assigned to ester groups at 1740 cm^{-1} (C=O ester symmetric stretch) and the emergence of a neighbouring band at 1710 cm^{-1} reflecting the concomitant formation of hydrogen-bonded carboxylic acid groups (C=O symmetric stretch of COOH). Based on the relative integrated absorbance of these bands, we infer that the yield of hydrolysis is ca. 40 %. Comparison of the IR spectra of the films **1-P** and **1-PH** in the CH and OH stretching region (2800-3800 cm^{-1}) shows that hydrocarbon chain remains unchanged, while there is no longer band corresponding to

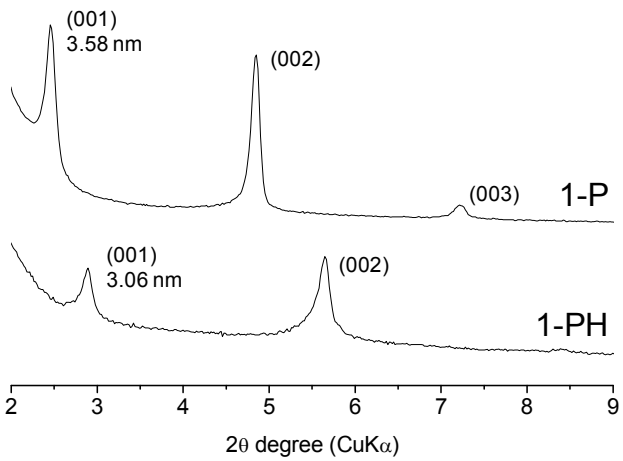

Figure 5. XRD patterns of the silsesquioxane films **1-P** (as-irradiated film derived from precursor **1**) and **1-PH** (after ester hydrolysis of film **1-P**).

residual hydrogen-bonded silanols (3400 cm^{-1}, stretch of the OH--O bonds), thus indicating further siloxane acid-catalysed condensation. The formation of acid protons and their possible engagement in hydrogen-bonding was investigated by ^{1}H MAS NMR based on the proton chemical shift. As shown in Figure 4, the spectrum of **1-PH** exhibits a distinctive acidic proton signal at ca. 11.2 ppm, assigned to the CO_2H protons, while absent before hydrolysis (**1-P**).[32] This resonance is the clear signature of hydrogen-bonded COOH groups, but its broadness may also suggest mixture of different hydrogen-bonded structures and the possibility of some free CO_2H groups (9 ppm). Furthermore, there is a relative decrease of the resonance attributed to the pendant methyl protons (CH_3O) of the ester group, slightly shifted downfield from 3.4 to 3.7 ppm after reaction. A hydrolysis degree of ca. 40 % was estimated by comparing the **1-P** and **1-PH** spectra, which is consistent with FTIR data. The increase in siloxane condensation during the ester hydrolysis step is also noticeable in the ^{1}H spectrum through the complete disappearance of hydrogen bonded SiOH protons (4.4 ppm).[33] The resonances of the aliphatic protons at ~1-2 ppm in the hydrolysed film (**1-PH**) are notably broader than those of the ester-functionalized film (**1-P**). The larger line width of the methylene protons (CH_2) may reflect a more rigid local environment due to higher level of condensation or/and enhanced hydrogen-bonding interactions among the COOH end groups. In contrast to ester groups, the carboxylic acid group can act as both a hydrogen-bond donor through the C-OH groups and an acceptor via the C=O oxygen, leading to a complex array of hydrogen bonds favoured by the head-to-head configuration of the lamellar mesostructure (Figure 2). As a result, the chain mobility of the carboxylic acid terminated silsesquioxane may be quite restricted, and approach that of a rigid crystalline solid. TGA data (see supporting information, Fig. S3) confirm that **1-PH** decomposes at higher temperature than **1-P**, respectively 520 and 460 °C for a weight loss of 50 %. The presumed H-bonded interactions engaged in the COOH-terminated film could provide the nanocomposite with better thermal stability.

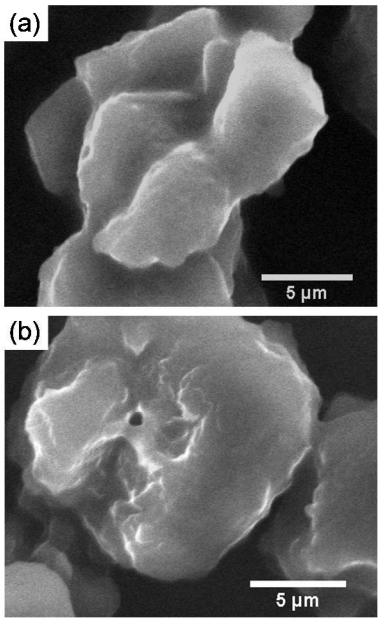

Figure 6. Representative SEM images of the scratched nanocomposite films **1-P** (**a**) and **1-PH** (**b**).

Figure 5 shows the result of ester hydrolysis on the XRD pattern of the nanocomposite film assembled from **1**, indicating clearly a conservation of the long-range ordered lamellar mesostructure. Nevertheless, hydrolysis caused a slight decrease in the d_{001}-spacing from 3.58 to 3.06 nm due to the end group shortening as well as the siloxane interlayer contraction induced by post-condensation reactions. Moreover, the exposure to a concentrated acid solution induced also greater disorder (one order of the 00*l* peaks was almost lost) along with some peak broadening. Although hydrolysis could be enhanced by a prolonged exposure to HCl solution, these conditions clearly affect the mesostructure stability. The hydrolysis conditions were chosen to ensure a trade-off between conversion and ordering. The SEM images in Figure 6 provide further evidence that the lamellar structure is retained. Even after the acid treatment, one can guess from the blurred images the same plate-like lamellar crystallites in the **1-P** and **1-PH** films.

3.2 Fluorescent micropattern: direct patterning using deep UV

The COOH-terminated silsesquioxane film (**1-PH**) represents a highly functional mesostructured support. Although accessibility may be lower than in surface reaction using SAMs, the multilayer structure provides a higher density of reactive groups and an enhanced robustness due to siloxane cross-linking. The reactive carboxylic acid functional groups found in the hybrid film **1-PH** allow it to be activated for attachment of amino ligands using standard method as that of 'normal' carboxylic acid group in organic chemistry. After immersion in a solution of a diamino fluorescent ligand (Safranin O, **L**), the resultant film (**1-PHL**) was washed several times with ethanol to remove the excess of dye non-specifically anchored to the silsesquioxane network. Binding was first

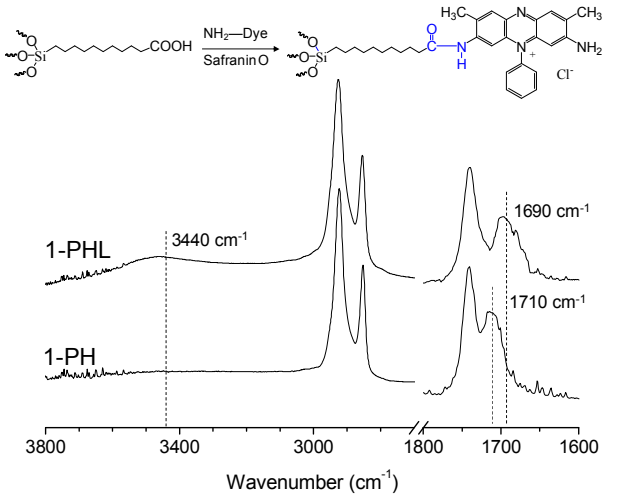

Figure 7. FTIR spectra of the COOH-functionalized hybrid film **1-PH** and **1-PHL** obtained after immersion in an ethanolic solution of **L**.

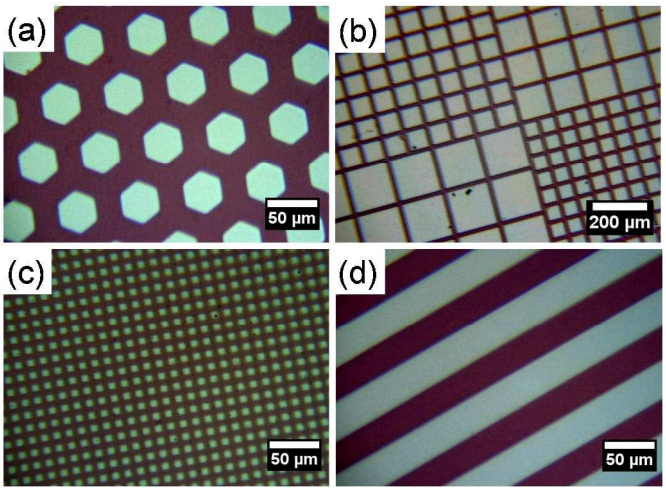

Figure 8. Optical microscopy images of the patterned **1-PHL** film obtained with different pattern feature size and shape: (a) hexagon; (b), mixed squares; (c), square; (d) bar (scale bar: 50 or 200 µm)

detected straightforwardly by optical and fluorescence microscopy (data not given). Additionally, we used FTIR spectroscopy to assess the yield of coupling. Figure 7 shows the IR spectra of the COOH-terminated hybrid to which the ligand **L** has been coupled. After activation, there is no band corresponding to residual carboxylic acid groups (C=O symmetric stretch of COOH, ≈ 1710 cm^{-1}), which are replaced entirely by another blue-shifted band of similar intensity assigned to NH-C(O) amide groups (C=O amide stretch ≈ 1690 cm^{-1}),[33] thus suggesting a quantitative coupling. Another evidence was given by the appearance of the characteristic ν(N-H) band at 3440 cm^{-1}. A benchmark experiment was performed by immersing a nonhydrolyzed film (**1-P**) in the same fluorescent ligand solution. As expected, the film remained transparent after washing and IR spectra revealed no sign of amide linkages or dye entrapment. We introduced finally a simple method to fabricate a fluorescent pattern based on the use of deep UV light directed through an optical mask deposited onto the **1-PHL** film surface. We used energetic photons to promote the spatially-controlled degradation of the organic fragments of the hybrid film exposed to UV light. After irradiation, the film was washed several times with acetone and ethanol, and the pattern was studied by optical and fluorescent microscopy. Figure 8 displays a series of optical images (a-d) of the patterned film prepared with masks of different shapes and sizes. The bright regions correspond to the irradiated areas, where the fluorescent and coloured ligand was degraded. In contrast, the red regions were masked and visibly preserved from calcination. Obviously, this direct photopatterning method allows the generation of precisely defined patterns of any arbitrary shape. Highly resolved micropatterns are achieved, and the smallest features that we have resolved are squares with a 7.5 µm side (Fig. 8c). The FTIR analysis (see supporting information, Fig. S4) of the irradiated areas reveals a complete cleavage of the amido bonds and a significant decrease of the C-H stretching modes (2800 and 3100 cm^{-1}) while the broad envelope (1000-1300 cm^{-1}) assigned to Si-O-Si antisymmetric stretching modes is unchanged. This result emphasizes a selective and partial removal of the organic components of the hybrid film but sufficient to fully quench the fluorescence. The consequence is a decreased thickness of ca. 400 nm in the exposed areas and the formation of well-resolved wells as evidenced by atomic force microscopy (see supporting information, Fig. S5). Additionally, the photogenerated pattern was investigated by fluorescence microscopy. Figure 9 shows the fluorescence emission image of the sample obtained with the hexagonal-shaped mask (Fig. 8a). Clearly, the honeycomb was successfully replicated. The non-exposed areas (bright yellow regions) outside the hexagons emit strong and uniform fluorescence signal, demonstrating the capacity of this process to access micropatterned fluorescence. The surface patterning of fluorescence molecules has found already a great importance in displays, optical memory devices and molecular switches, as well as in the sensor and imaging industries.[34-36]

4. Conclusions

Carboxylic acid terminated monolayers have already demonstrated their potential as reactive surface in covalent immobilization of biomolecules, electrochemistry, and crystal growth. In this report, we have described a UV methodology to create COOH-functionalized silsesquioxane films possessing a highly ordered multilayer mesostructure. The method required the photoacid-catalysed sol-gel process of ester-terminated alkoxysilane **1**. Subsequent ester hydrolysis by HCl treatment allowed their conversion into carboxylic acid terminal groups as demonstrated by FTIR and solid state ^{1}H MAS NMR (yield: 40 %). A combination of XRD and SEM ensured that this chemical reaction was not accompanied by a loss of the initial mesostructure. The resultant COOH-functionalized represented a suitable platform for quantitative coupling of amino ligands such as Safranin O. High quality fluorescence micropatterns

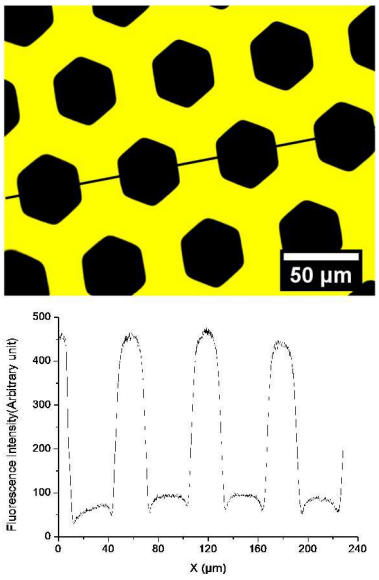

Figure 9. Image of the photopatterned **1-PHL** film surface obtained with fluorescence microscopy (scale bar = 50 µm).

were achieved using a UV degradation photolithography procedure.

By successfully adapting this technique to the immobilization and patterning of biologically active amino-reactive ligands for instance, there exists significant potential to study cell adhesion and spreading, biofouling mechanism, or the elaboration of bioanalytical devices (biosensors, protein biochips, miniaturization of DNA analyses).[37, 38] We believe that micrometer-scale ordered film structure have several advantages over molecular-scale monolayers based on chloro- or alkoxysilane including higher functionality, potential applicability on a variety of substrates without particular surface preparation and chemical/mechanical resistance because of the cross-linked siloxane interlayers.

Notes and references

[a] Laboratory of Photochemistry and Macromolecular Engineering, ENSCMu, University of Haute-Alsace, 3 bis rue Alfred Werner 68093 Mulhouse Cedex, France.
[b] Institute of Material Science of Mulhouse, CNRS, UMR 7361, University of Haute-Alsace, 3 bis rue Alfred Werner 68093 Mulhouse Cedex, France.
[c] Laboratory of Modelling, Intelligence, Process and Systems, ENSISA, University of Haute-Alsace, 61 rue Albert Camus, 68093 Mulhouse Cedex, France.
[d] Key Laboratory for Palygorskite Science and Applied Technology of Jiangsu Province, College of Bioengineering and Chemical Engineering, Huaiyin Institute of Technology, Huaian 223003, People's Republic of China.

*Corresponding authors:
Dr. Abraham Chemtob; e-mail: abraham.chemtob@uha.fr; Tel: +33 3 8933 5030; Fax: +33 3 8933 5017.
Dr. Lingli Ni; e-mail: nilingli520@126.com; Tel: +86 517 83559056; Fax: +86 517 83559056.

Electronic Supplementary Information (ESI) available: []. See DOI: 10.1039/b000000x/

1. C. Sanchez, P. Belleville, M. Popall and L. Nicole, *Chem. Soc. Rev.*, 2011, **40**, 696-753.
2. C. Sanchez, C. Boissière, S. Cassaignon, C. Chaneac, O. Durupthy, M. Faustini, D. Grosso, C. Laberty-Robert, L. Nicole, D. Portehault, F. Ribot, L. Rozes and C. Sassoye, *Chem. Mater.*, 2014, **26**, 221-238.
3. A. Mehdi, C. Reyé and R. J. P. Corriu, *Chem. Soc. Rev.*, 2011, **40**, 563-574.
4. S. Fujita and S. Inagaki, *Chem. Mater.*, 2008, **20**, 891-908.
5. M. Barboiu, *Chem. Commun.*, 2010, **46**, 7466-7476.
6. N. Mizoshita, T. Tani and S. Inagaki, *Adv. Funct. Mater.*, 2011, **21**, 3291-3296.
7. E. Besson, A. Mehdi, A. Van der Lee, H. Chollet, C. Reye, R. Guilard and R. J. P. Corriu, *Chem. Eur. J.*, 2010, **16**, 10226-10233.
8. X. Sallenave, O. J. Dautel, G. Wantz, P. Valvin, J.-P. Lère-Porte and J. J. E. Moreau, *Adv. Funct. Mater.*, 2009, **19**, 404-410.
9. A. Chemtob, L. Ni, C. Croutxé-Barghorn and B. Boury, *Chem. Eur. J.*, 2014, **20**, 1790-1806.
10. B. Boury and R. J. P. Corriu, *Chem. Rec.*, 2003, **3**, 120-132.
11. A. Shimojima and K. Kuroda, *Chem. Rec.*, 2006, **6**, 53-63.
12. J. J. E. Moreau, L. Vellutini, M. Wong Chi Man, C. Bied, J. L. Bantignies, P. Dieudonné and J. L. Sauvajol, *J. Am. Chem. Soc.*, 2001, **123**, 7957-7958.
13. S. C. Nunes, N. J. O. Silva, J. Hummer, R. A. S. Ferreira, P. Almeida, L. D. Carlos and V. De Zea Bermudez, *RSC Adv.*, 2012, **2**, 2087-2099.
14. N. Liu, K. Yu, B. Smarsly, D. R. Dunphy, Y.-B. Jiang and C. J. Brinker, *J. Am. Chem. Soc.*, 2002, **124**, 14540–14541.
15. H. Peng, J. Tang, J. Pang, D. Chen, L. yang, H. S. Ashbaugh, C. J. Brinker, Z. Yang and Y. Lu, *J. Am. Chem. Soc.*, 2005, **127**, 12782-12783.
16. Y. Luo, J. Lin, H. Duan, J. Zhang and C. Lin, *Chem. Mater.*, 2005, **17**, 2234-2236.
17. M. Barboiu, S. Cerneaux, A. van der Lee and G. Vaughan, *J. Am. Chem. Soc.*, 2004, **126**, 3545-3550.
18. L. Yang, H. Peng, K. Huang, J. T. Mague, H. Li and Y. Lu, *Adv. Funct. Mater.*, 2008, **18**, 1526-1535.
19. J. Alauzun, A. Mehdi, C. Reye and R. J. P. Corriu, *J. Am. Chem. Soc.*, 2005, **127**, 11204-11205.
20. J. Alauzun, E. Besson, A. Mehdi, C. Reyé and R. J. P. Corriu, *Chem. Mater.*, 2008, **20**, 503-513.
21. J. Alauzun, A. Mehdi, C. Reyé and R. J. P. Corriu, *Chem. Commun.*, 2006, 347-349.
22. R. Mouawia, A. Mehdi, C. Reyé and R. J. P. Corriu, *J. Mater. Chem.*, 2007, **17**, 616-618.
23. R. Mouawia, A. Mehdi, C. Reyé and R. J. P. Corriu, *J. Mater. Chem.*, 2008, **18**, 2028-2035.
24. J. H. El-Nakat, N. Al-Hakim, S. Habib, P. Obeid, M.-J. Zacca, G. Gracy, S. Clement and A. Mehdi, *J. Inorg. Organomet. Polym Mater.*, 2014, **24**, 508-514.
25. A. Boullanger, G. Gracy, N. Bibent, S. Devautour-Vinot, S. Clément and A. Mehdi, *Eur. J. Inorg. Chem.*, 2012, **2012**, 143-150.
26. A. Chemtob, L. Ni, A. Demarest, C. Croutxé-Barghorn, L. Vidal, J. Brendlé and S. Rigolet, *Langmuir*, 2011, **27**, 12621-12629.
27. L. Ni, A. Chemtob, C. Croutxé-Barghorn, L. Vidal, J. Brendlé and S. Rigolet, *J. Mater. Chem.*, 2012, **22**, 643 - 652.
28. L. Ni, A. Chemtob, C. Croutxé-Barghorn, J. Brendlé, L. Vidal and S. Rigolet, *J. Phys. Chem. C*, 2012, **116**, 24320–24330.

29.J. Lahiri, E. Ostuni and G. M. Whitesides, *Langmuir*, 1999, **15**, 2055-2060.
30.P. Jonkheijm, D. Weinrich, H. Schroder, C. M. Niemeyer and H. Waldmann, *Angew. Chem. Int. Ed.*, 2008, **47**, 9618 – 9647.
31.H. De Paz, A. Chemtob, C. Croutxé-Barghorn, S. Le Nouen and S. Rigolet, *J. Phys. Chem. B*, 2012, **116**, 5260-5268.
32.S. Pawsey, M. McCormick, S. De Paul, R. Graf, Y. S. Lee, L. Reven and H. W. Spiess, *J. Am. Chem. Soc.*, 2003, **125**, 4174-4184.
33.J. B. D. delaCaillerie, M. R. Aimeur, Y. ElKortobi and A. P. Legrand, *J. Colloid Interface Sci.*, 1997, **194**, 434-439.
34.M. Irie, T. Fukaminato, T. Sasaki, N. Tamai and T. Kawai, *Nature*, 2002, **420**, 759-760.
35.M. Melucci, M. Zambianchi, L. Favaretto, V. Palermo, E. Treossi, M. Montalti, S. Bonacchi and M. Cavallini, *Chem. Commun.*, 2011, **47**, 1689-1691.
36.S.-Y. Ku, K.-T. Wong and A. J. Bard, *J. Am. Chem. Soc.*, 2008, **130**, 2392-2393.
37.G. M. Whitesides, E. Ostuni, S. Takayama, X. Y. Jiang and D. E. Ingber, *Annu. Rev. Biomed. Eng.*, 2001, **3**, 335-373.
38.T. Ekblad and B. Liedberg, *Curr. Opin. Colloid Interface Sci.*, 2010, **15**, 499-509.

